Graphene as Thin Film Infrared Optoelectronic Sensor

Gilgueng Hwang[1], Juan Camilo Acosta[1], Emir Vela[1,2], Sinan Haliyo[1], Stéphane Régnier[1]

[1]Insitut des Systèmes Intelligents et de Robotique
Université Pierre et Marie Curie, CNRS UMR7222, BC173
4 Place Jussieu, F-75005 Paris, France
[2]CEA LIST, Sensory Interfaces Laboratory
18, route du Panorama, BP6, Fontenay aux Roses, F-92265, France
hwang@isir.fr

Abstract—**We present the conductometric behavior of a single atomic carbon nanostructure (graphene) that could be promising to infrared optoelectronic applications. A graphene nanomanipulation system with focused infrared laser source for optoelectronic property characterizations is implemented. The feasibility of mechanical and electrical probing manipulations on two-dimensional thin film nanostructures is studied. Using this system, we revealed the infrared optoelectronic properties of mono- and multilayer graphene. The obtained optoelectronic parameters are compared to the single- and multi-walled nanotubes. A graphene infrared sensor is prototyped by direct writing of electrodes using gold nanoink fountain-pen method and is analyzed by electrical probing. Results show that graphene could be a promising building block for thin film optoelectronic devices.**

Keywords-component; graphene; infrared optoelectronics; nanomanipulation; conductometric; photoconductivity; temperature dependence

I. INTRODUCTION

Various two-dimensional nanostructures have been synthesized from different materials. Graphene is the newest member in two-dimensional (2D) carrier systems, which have shown a spectrum of fascinating new physics and consequently draw much attention [1,2]. Graphene is a single layer of honeycomb carbon lattice, the atomic sheet of graphite that represents the ultimate 2D material. Graphene was extensively studied on electrical transport but not much on optical investigations. Such an optical study is important to understand the electronic structures and excited-state properties of low-dimensional materials, as was demonstrated in carbon nanotubes [3]. Especially, Infrared (IR) spectroscopy was shown to reveal the Landau Level (LL) spectrum when combined with a magnetic field [4,5]. We could also envision new possibilities of graphene based optoelectronic sensors and their application to nanoelectromechanical systems (NEMS).

Recently, temperature dependence of graphene resistivity was studied [6-8]. Optical properties of graphene were also studied for the optoelectronic applications but were limited to the gate triggered optical transitions [9,10]. However, investigations of IR optical properties of graphene are still missing and devices based on these nanostructures have not been created yet.
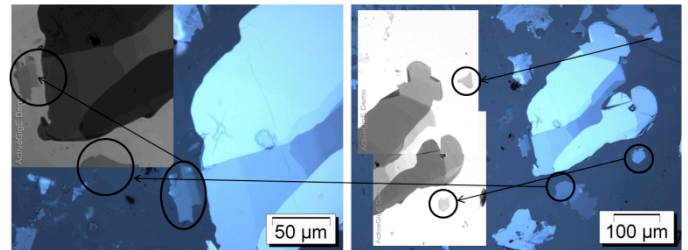

Fig. 1 Graphene sample prepared over glass substrate: the insets display photos taken from the inverted microscope used in this experiment.

This paper presents the electrical probing of optoelectronic properties of mono- and multilayer graphene and their use as conductometric sensors to detect IR laser. First, our nanorobotic manipulation setup is described. Then, conductometric properties of graphene in IR are characterized. Finally, direct writing of conductometric IR sensor with fountain-pen based gold nanoink deposition is demonstrated.

II. GRAPHENE NANOMANIPULATION

A. Graphene on Glass

A graphene sample was prepared onto the glass Pyrex substrate using the process described in the reference [11]. The sample preparation was inspired from the anodic bonding that is usually used to bond Si to a Pyrex substrate. Very firm contact is obtained between the substrate and Si allowed by the formation of chemical bonds at the interface by an application of a potential difference on the order of a kV to the heated Pyrex/Si substrate. The principle of anodic bonding in Si/Pyrex can further be referred from the [11].

The similar mechanism was applied to the conducting materials that readily oxidize to bond to Pyrex substrates. An anodic voltage (1.2 ~ 1.7kV) was applied on the graphite sample with the cathode contacting the backside of the Pyrex substrate. The substrate was heated to around 200°C. After the bonding is achieved, the bulk graphite sample can be cleaved off, leaving several bonded areas on the glass surface. These are then peeled off using adhesive tape to leave many transparent areas with mono-/multilayer (layer configuration) graphene. Optical microscopy was used to pre-identify the

graphene layer configurations from the reference contrast as shown in Fig. 1.

Further Raman spectroscopy identification of different contrasts in different graphene layer configurations can be referred from the paper [11] thus it is not described here.

Large area, high quality graphene sample was prepared for the conductometric property characterizations using this simple and low-cost method.
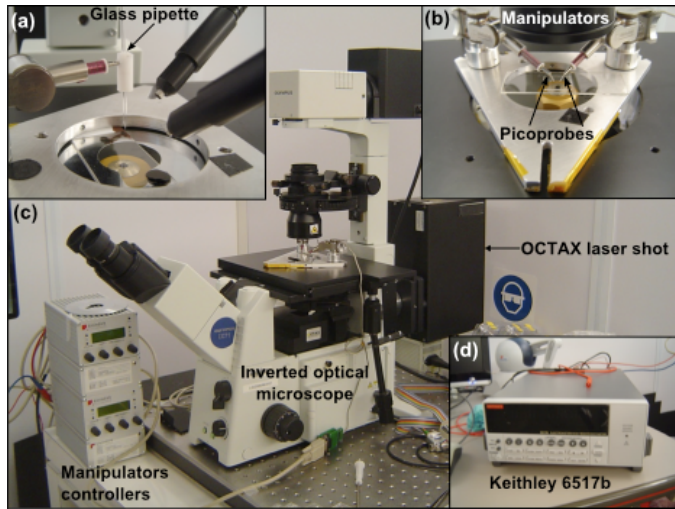

Fig. 2 Graphene nanomanipulation setup on inverted optical microscope: (a) fountain-pen based gold nanoink deposition setup (additional two light sources are utilized instead of built-in one to have more vertical space), (b) micromanipulators for electrical probing and mechanical manipulation, (c) piezo controller for micromanipulators, and (d) high resistance measurement unit

B. Graphene Nanomanipulation System

The platform setup is composed of an inverted Olympus IX71 microscope (Fig. 2), with a 25x OCTAX objective and a high speed Dalsa Genie CMOS camera (1", 1400 x 1024 pixels, 60fps). An infrared (IR) laser (CW 1480nm, max power of 120 mW) from OCTAX Microscience GmbH is connected to the rear port of the microscope. The focused laser spot diameter is approximately 1μm.

For the fountain-pen based gold nanoink deposition, a single Kleindiek (MM3A-EM) manipulator was used (Fig. 2a). For probing and manipulating graphene, two of the same manipulators were used (Fig. 2b). Each has 3 degrees of freedom and respectively 5 nm, 3.5nm and 0.25 nm resolution at the tip in X, Y and Z axis of inertial frame. Each axis is actuated with piezo stick-slip principle and is controlled via a piezo controller (Fig. 2c). The current between two probes of manipulators could be measured with a low-current electrometer (Keithley 6517b) by the application of a voltage across them (Fig. 2d).

The graphene nanomanipulation setup shown in the Fig. 2 has several functions including electrical probing, focused laser setup, gold nanoink deposition, and mechanical manipulation.

(a) Substrate

(b) Manipulator picoprobes

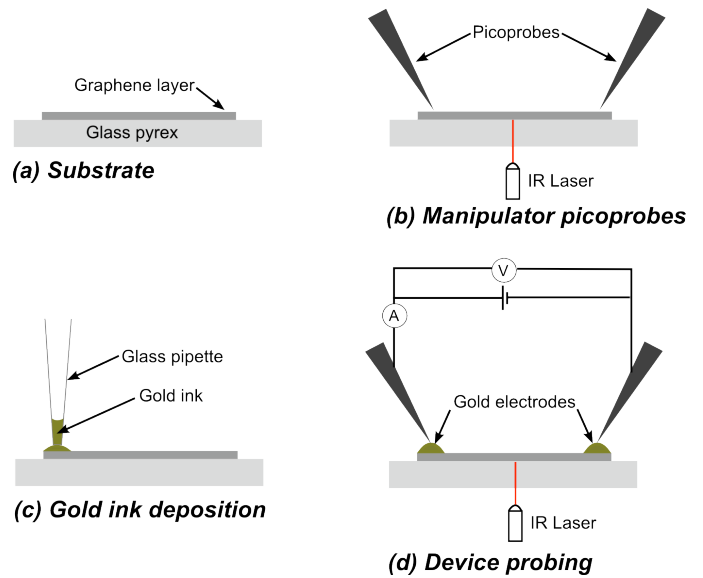(c) Gold ink deposition

(d) Device probing

Fig. 3 Schematic of graphene device assembly: (a) attach the graphene layer on top of the transparent Pyrex glass surface, (b) electrical probing by 2 picoprobes and IR laser, (c) deposit gold nanoink to create electrodes, (d) finally, connect the picoprobes to the electrodes, the power supply, and the electrometer for current and voltage monitoring under IR laser.

C. Process Summary

Schematic of graphene electrical probing and sensor fabrication is described here. First the graphene layer is prepared on top of the transparent Pyrex glass surface and imaged using the inverted microscope (Fig. 3a). This setup has proved to be useful for manipulation mainly because of transparent optical characteristics of graphene layer and enough space to install manipulators on top of the microscope sample stage. Then 2 picoprobes mounted to the Kleindiek manipulators are used to characterize electrical transport properties of the graphene sample (Fig. 3b). A metal probe (Picoprobe, T-4-10-1 mm, tip radius: ~100nm) mounted on the nanomanipulator was used. Thirdly the gold electrode is created by fountain-pen based gold nanoink deposition. Once the graphene layer is electrically characterized, the fountain-pen method was used to pattern the electrodes [14] (Fig. 3c).

For the gold nanoink deposition, a borosilicate capillary was pulled to make a tapered micropipette with 1μm diameter outer tip. Since the graphene surface is hydrophobic, both mechanical force and back pressure are combined to deposit droplets. Finally, the chip is placed onto a hotplate and heated to 350°C and annealed for 45 minutes to assure an ohmic contact. Conductivity improvement after deposition was reported in previous works with thin film structures [15,16]. Finally, the picoprobes are put in contact with the electrodes for current and voltage monitoring with the Keithley 6517b under the focused laser source (Fig. 3d).
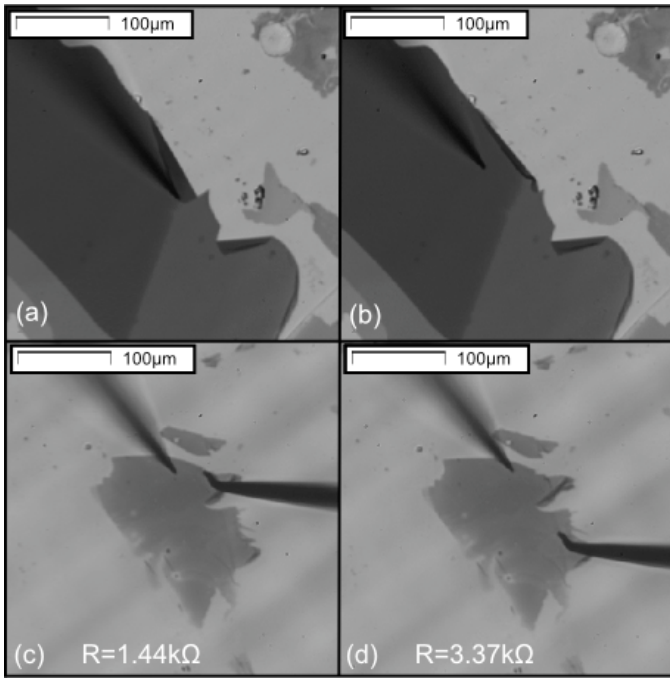
Fig. 4 Graphene manipulation using the proposed setup: (a,b) mechanical pushing and pulling of graphene, (c,d) electrical probing.
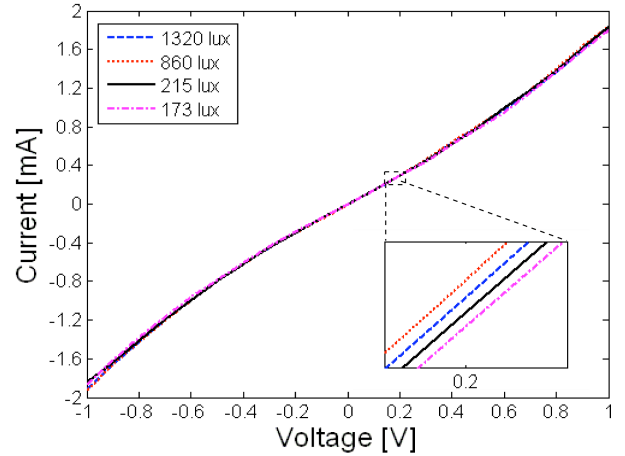

Fig. 5 Photoconductivity measurements of graphene with a visible light source (calibrated as 173, 215, 860, and 1320 lux). The inset figure was zoomed at 0.2V.

D. Graphene Nanomanipulation

The implemented setup is tested to prove the feasibility to manipulate the graphene layer. Graphene pushing and pulling show that our setup is adequate for such manipulations (Fig. 4a,b). The whole process can be monitored using the inverted optical microscope. It allows better manipulation with good quality visual feedback, which helps to avoid the excessive force that might break the sample.

Contact resistance of graphene during electrical probing could be estimated (Fig. 4c,d). The transmission line model (TLM) was utilized while probing with the above-described method. The measured total resistance of graphene at 1V was from 1.44kΩ to 3.37kΩ depending on the distance between two probes. This range is similar to resistance of intrinsic bilayer graphene from other sources in literature [11-13].

From the TLM analysis, the contact resistance was estimated as around 400Ω at 1V which could further be reduced by patterning gold electrodes and probing directly onto them [17]. It should also be noted that contact resistance was kept constant at the same potential during the conductometric experiments. Therefore, we can estimate intrinsic graphene resistance by simply subtracting contact resistance.

The manipulation setup described here is proved to be useful to the mechanical and electrical probing manipulations of all two-dimensional ultra-thin film transparent structures and it is not limited to graphene.

III. CONDUCTOMETRIC PROPERTIES OF GRAPHENE

A. Photoconductive Behavior in Visible Light

The graphene photoconductivity was characterized under the ambient environment to pinpoint the effect from a visible light source.

First, the multilayer graphene samples were characterized in their photoconductive behavior. The I-V characteristics were recorded from -1V to 1V with voltage steps of 0.1V (Fig. 5). The repeatable nonlinear I-V characteristics were observed in the range from |0.2V| to |1V| that was not clearly mentioned in other sources [11-13]. It can be explained by a slight decrease of contact resistance at relatively higher potential regions (0.2 ~ 1V). This effect can be avoided by gold electrode patterned onto the graphene with ohmic conductivity. However, a more detailed investigation is required to understand this phenomenon.

The optical microscope light source (visible light with wavelength around 600nm) was utilized for the experiment and was calibrated with a lux meter. The measured light intensity was 173, 215, 860, and 1320 lux. For each light source, the I-V curves were recorded and are plotted in Fig. 5.

There was no clear photoconductive behavior of graphene with a visible light source (Fig. 5). This is expected as the graphene layer is transparent under visible light wavelengths thus do not absorb photons to trigger any photoconductivity. Since both monolayer and multilayer graphene are not good photoconductors because of their ultra-transparency under ambient light source, they could be featured as future electronic components less sensible to environmental effects. For the optoelectronics applications of graphene, we then further investigated its IR photoconductive behavior.
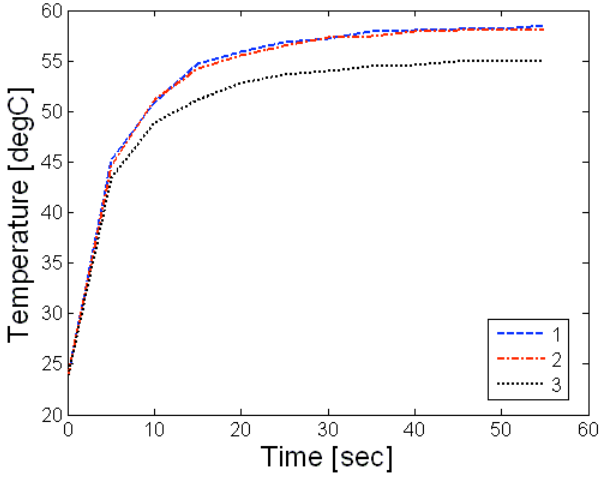
Fig. 6 Temperature calibration of the focused laser: graphene can be heated from 24 to 60°C. The numbers in legend and the according to lines depict the trial times.

B. Infrared (IR) Light Detection

In order to investigate light wavelength selectivity of graphene, its photoconductivity in respect to IR response and temperature is analyzed.

As the graphene layer is extremely thin and transparent, a focused laser beam is used to heat it up through the inverted microscope. To distinguish the effect from temperature dependence of graphene, temperature calibration of laser heating was performed with the Keithley 6517b and its thermocouple prior to the measurement of IR photoconductivity. The thermocouple probe was placed onto the fresh glass substrate on top of the inverted microscope sample stage. Then the IR laser source was turned on to heat up the sample while measuring simultaneously the temperature. The recorded data in repeated laser switch on and off was shown in Fig. 6. Because of the limited power of laser source (120mW) and the size of the focused area (1μm) through magnified lens objective, temperature was saturated at around 60°C.

Fig. 7 shows the I-V characteristics of graphene during the laser switch on and off. Compared to studies in literature that report increasing resistivity of graphene over temperature [6-8], we measured a decrease in resistivity that consequently increases the conductivity when the laser source is on. Our hypothesis is that the increase of resistivity because of the temperature rise is largely compensated by its decrease under IR laser. Thus photon effect should be discussed.

We further analyzed the absorbed IR gated transport behavior. The notion of normalized change of IR reflectivity - $\delta R/R$ versus photon energy for a representative graphene monolayer and bilayer can be applied. Note that $-\delta R/R$ is related to the complex optical conductivity $\sigma\ (\omega)$ of graphene through the relation [9]:

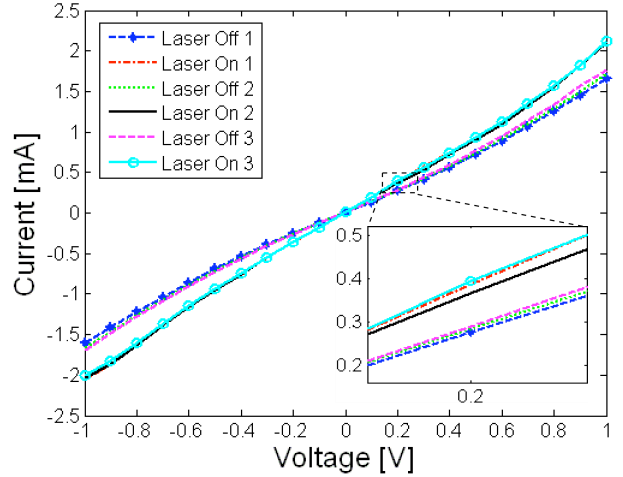$$-\frac{\delta R}{R} = \frac{1}{c}\text{Re}\big[\eta \cdot \sigma\big] \qquad (1)$$

Fig. 7 IR detection was shown with the multilayer graphene I-V characteristics: the I-V curves are recorded by the iterative laser switching on and off. Resistance decreases when the laser is on. The inset figure is a zoom at 0.2V.

where η is a dimensionless complex factor that includes an interfering contribution from substrate reflection and can be calculated exactly. Therefore, the increased conductivity when the applied IR laser is attributed to the increased reflectivity from Eq. (1). This different electrical transport phenomena of graphene with different optical reflectivity is to be discussed more in detail in Section 3.C.

The IR triggered conductivity change of graphene is coupled between the positive temperature dependence and reflectivity effect. Furthermore, the graphene conductance was found to be dominated by IR reflectivity change in temperature region between 24~60°C. The selective wavelength absorption in graphene was revealed in IR range.

C. Thickness Dependence

The relation between graphene layer thickness and as-described IR photoconductivity is not known. Therefore it should be more investigated with different layer configurations during the electrical transport measurements. This on-spot IR profiling feature is practical especially to identify and to confirm pre-identified graphene layer configurations during electrical probing.

Thickness (numbers of layers) dependence of graphene versus the electrical transport property was measured to reveal the different behaviors of IR photoconductivity. This phenomenon is mainly attributed to the difference of IR reflectivity in different layer configurations (mono- and multilayer graphene).

Fig. 8 shows the measured I-V curves of monolayer and multilayer graphene. The inset photos of Fig. 8 depict how two probes are measuring the electrical property through different layer configurations. Three different configurations of electrical probing were tested to obtain optoelectronic parameters of their different IR photoconductivity.
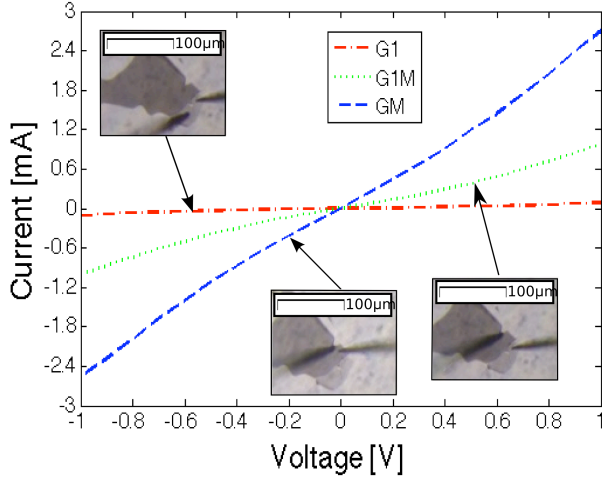
Fig. 8 Layer thickness dependence of multilayer graphene I-V characteristics: the I-V curves are recorded in three different probing configurations: monolayer, multilayer, and between them. The IR optoelectronic behavior was measured by the iterative laser switching on and off. G1, GM, and G1M describe graphene monolayer, multilayer and between them.

It can be summarized as the probing on monolayer, multilayer, and between them. The resistivity was higher in monolayer graphene than in multilayer case although the same IR photoconductive behaviors were observed.

To compare the IR photoconductive behavior in different layer configurations (monolayer and multilayer) one measured graphenes and multi- and single-walled carbon nanotubes (MWCNT and SWCNT), the EQE (external quantum efficiency) of the detector was used [18].

The linear regions of I-V characteristics were shown in -0.2V ~ 0.2V range from the results (Fig. 5,7 and 8). We also estimated the energy conversion efficiency (η) of the graphene. $\eta = P_{el}/P_{in}$, where $P_{el} = dI \times V_{bias}$ and P_{in} is the power intensity of infrared laser. We further estimated the performance of the graphene IR photoconductor including its responsiveness. The maximum theoretical values of EQEs of the detectors are depend on several parameters such as responsiveness and light absorption wavelength (Eq. (2)).

$$Q = 100 \times R_d \times (1.2395/\lambda) \qquad (2)$$

where $Q(\%)$, $R_d(A/W)$, and $\lambda(\mu m)$ are EQE, responsiveness, and wavelength of light source respectively. We further evaluated the responsiveness of graphene IR photodetection ($R_d(A/W) = dI/P_{in}$) where the (dI) is photocurrent per unit power intensity (P_{in}), and EQE (%) described in Eq. (2).

Table 1 summarizes the obtained parameters of graphene and compares them with as-studied parameters of single-, double-, and multi-walled nanotubes (SWNTs, DWNTs, and MWNTs) [18].
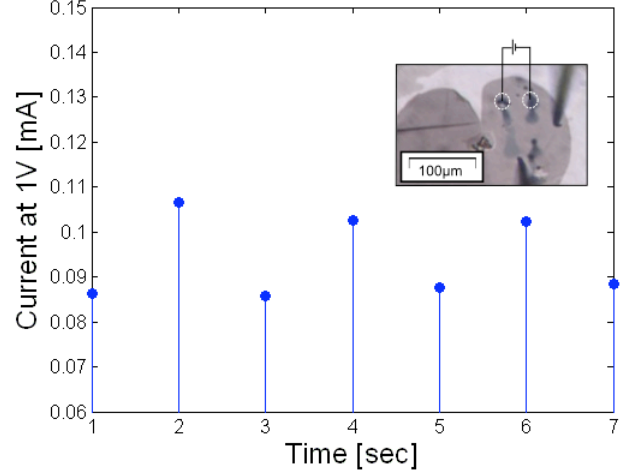

Fig. 9 Repeatable (3 times of switching on and off IR laser) measurement of IR photoconductive sensor using monolayer graphene and direct gold nanoink written electrodes.

The responsiveness of multilayer graphene at 1V (voltage source) is measured as 3.634 mA/W that is more than 16 times higher than the one of monolayer (0.222 mA/W). It should be noted that in literature [18] MWNTs has shown less responsiveness than SWNTs which is contrary to our measurements in graphene. This can be explained by the fact that more complicated optical reflection and scattering through the tube type carbon structures interrupt their original IR optoelectronic transport of 2-D graphene. However, the excitation through the transparent graphene layers is purely attributed to a dramatic increase in photon–conductivity behavior with multiple layers.

Table 1. Optoelectronic parameters such as energy conversion efficiency (η), responsiveness (R_d), and external quantum efficiency (Q) of graphene monolayer (G1), multilayer (GM) and between them (G1M): SNT (single-walled nanotube), DNT (double-walled nanotube), and MNT (multi-walled nanotube), the data of SNT, DNT, and MNT are from [16]. P_{in}, V_b, dI, and P_{el} are respectively the unit power intensity, the bias voltage, the photocurrent, and the generated power intensity by photocurrent.

	P_{in} (W)	V_b (V)	dI (μA)	P_{el} (μW)	η(%)	R_d (mA/W)	Q (%)
G1	0.12	1	2.7	2.7	0.02	0.2	0.02
GM	0.12	1	417	417	0.36	3.6	0.35
G1M	0.12	1	401	401	0.33	3.3	0.28
SNT	0.08	1	136	136	0.18	1.8	0.22
DNT	0.13	1	407	407	0.13	1.27	0.15
MNT	0.19	0.05	144	7.2	0.004	0.76	0.09

There are also dramatic differences between the observed spectra of graphene monolayer and multilayer. The graphene monolayer spectrum is featureless, which is consistent with the linear electronic bands. In fact, the absorption coefficient of an undoped graphene layer in the IR region is expected to

be strictly constant. The bilayer graphene electronic structure exhibits a clear peak around 350 meV, near the parallel band separation of 400 meV determined by photoemission [9].

In above-described study, the negative IR photoresistive behavior of mono- and multilayer graphene was characterized. The layer thickness was related to the responsiveness that can be useful to identify the layer configurations in mono-/multilayers that differs from the one in nanotubes. This can be utilized for profiling layer thickness by monitoring I-V characteristics with resistivity and the according transition of responsiveness.

IV. GRAPHENE CONDUCTOMETRIC SENSORS

A. Infrared Laser Optic Sensors

To prototype the graphene IR sensors, fountain-pen based gold nanoink deposition was used. The maskless writing of the gold electrodes over the graphene layer was achieved using the process described in the Section 2. Electrodes patterned onto monolayer graphene with gold nanoink are depicted in the inset of Fig. 9. The repeatable current switching behavior through the graphene was observed when the IR laser was turned on and off. The gold nanoink deposition method is proved to be a simple and low-cost way to create graphene based two-dimensional devices.

Furthermore, the created graphene thin film IR sensors with the feature of direct and simple layer configuration profiling is promising to further detailed electrical transport phenomena of graphene by Hall study and etc.

V. CONCLUSIONS

A high quality large area graphene sample was prepared for conductometric property characterizations and manipulation using a simple and low-cost method. The negative IR photoresistive behavior of mono- and multilayer graphene with different resistivity were clearly characterized using micromanipulators installed onto an inverted optical microscope. It is also found that the layer thickness of graphene was related to the responsiveness of IR photoconductivity. This can be used for direct profiling of layer configurations to identify mono-/multilayer configurations based on their resistivity difference. The simplicity of the obtained optoelectronic parameters of graphene is attributed mainly to their perfect 2-D structures and the quality of the sample, which explains the difference from both SWNTs and MWNTs. Finally, the fountain-pen based gold nanoink deposition method was successfully applied to write 2-D graphene IR detectors over Pyrex glass without using any cleanroom microfabrication processes which could be promising to reduce the manufacturing cost. The revealed optoelectronic properties of graphene in IR region and maskless simple device prototype methods could promisingly open to more applications in both optics and optomechatronics fields.

ACKNOWLEDGMENTS

REFERENCES

[1] K. S. Novoselov, A. K. Geim, S. V. Morozov, D. Jiang, Y. Zhang, S. V. Dubonos, I. V. Grigorieva, and A. A. Firsov, "Electric field effect in atomically thin carbon films", Science, vol. 306, 2004, pp. 666-669

[2] K. S. Novoselov, A. K. Geim, S. V. Morozov, D. Jiang, M. I. Katsnelson, I. V. Grigorieva, S. V. Dubonos, A. A. Firsov, "Two-dimensional gas of massless dirac fermions in graphene", Nature, vol. 438, 2005, pp. 197-200

[3] S. M. Bachilo, M. S. Strano, C. Kittrell, R. H. Hauge, R. E. Smalley, R. B. Weisman, "Structure-assigned optical spectra of single-walled carbon nanotubes", Science, vol. 298, 2002, pp. 2361-2366

[4] Z. Jiang, E. A. Henriksen, L. C. Tung, Y. J. Wang, M. E. Schwartz, M. Y. Han, P. Kim, and H. L. Stormer, "Infrared spectroscopy of landau levels of graphene", Phys. Rev. Lett., vol. 98, 2007, pp. 197403

[5] D. Abergel, and V. Falko, "Optical and magneto-optical far-infrared properties of bilayer graphene", Phys. Rev. B, vol. 75, 2007, pp. 155430

[6] K. I. Bolotin, K. J. Sikes, J. Hone, H. L. Stormer, and P. Kim, "Temperature-dependent transport in suspended graphene", Phys. Rev. Lett., vol. 101, 2008, pp. 096802

[7] W. Xu, F. M. Peeters, and T. C. Lu, "Dependence of resistivity on electron density and temperature in graphene", Phys. Rev. B, vol. 79, 2009, pp. 073403

[8] A. Akturk and N. Goldsman, "Unusually strong temperature dependence of graphene electron mobility", Proc. Intl. Conf. on Simulation of Semiconductor Processes and Devices, 2008, pp. 173-176

[9] F. Wang, Y. Zhang, C. Tian, C. Girit, A. Zettl, M. Crommi, and Y. R. Shen, "Gate-variable optical transition in graphene", Science, vol. 320, 2008, pp. 206-209

[10] D. Prezzi, D. Varsano, A. Ruini, A. Marini, and E. Molinari, "Optical properties of graphene nanoribbons: the role of many-body effects", Phys. Rev. B, vol. 77, 2008, pp. 041404

[11] A. Shukla, R. Kumar, J. Mazher, and A. balan, "Graphene made easy: high quality, large-area samples", Solid State Comm., vol. 149, 2009, pp. 718-721

[12] A. Das, S. Pisana, B. Chakraborty, S. Piscanec, S. K. Saha, U. V. Waghmare, K. S. Novoselov, H. R. Krishnamurthy, A. K. Geim, A. C. Ferrari, and A. K. Sood, "Monitoring dopants by raman scattering in an electrochemically top-gated graphene transistor", Nature Nanotech., vol. 3, 2008, pp. 210-215

[13] J. B. Oostinga, H. B. Heersche, X. Liu, A. F. Morpurgo, and L. M. K. Vandersypen, "Gate-induced insulating state in bilayer graphene devices", Nature Materials, vol. 7, 2008, pp. 151-157

[14] C. P. R. Dockendorf, M. Steinlin, T. Choi, D. Poulikakos, "Individual carbon nanotube soldering with gold nanoink deposition", Appl. Phys. Lett., vol. 90, 2007, pp. 193116

[15] C. P. R. Dockendorf, G. Hwang, C. P. Grigoropoulos, B. Nelson, and D. Poulikakos, "Maskless writing of a flexible nanoscale transistor with Au-contacted carbon nanotube electrodes", Appl. Phys. Lett., vol. 91, 2007, pp. 243118

[16] G. Hwang, C. Dockendorf, D. Bell, L. Dong, H. Hashimoto, D. Poulikakos, B. Nelson, "3-D InGaAs/GaAs helical nanobelts for optoelectronic devices", Intl. J. Optomech., vol. 2, 2008, pp. 88-103

[17] Schroder, D. K. Semiconductor Material and DeVice Characterization; John Wiley & Sons Inc.: New York, 2006

[18] J. Wei, J. Sun, J. Zhu, K. Wang, Z. Wang, J. Luo, D. Wu, and A. Cao, "Carbon nanotube macrobundles for light sensing", Small, vol. 2, 2006, pp. 988-993